Int. J. Solids Structures, 1973, Vol. 9, pp. 461 to 480. Pergamon Press. Printed in Great Britain

AXIALLY SYMMETRIC TRANSIENT WAVE PROPAGATION IN ELASTIC RODS WITH NONUNIFORM SECTION

P. C. Y. LEE† and Y. S. WANG

Department of Civil and Geological Engineering, Princeton University, Princeton, New Jersey

Abstract—A one-dimensional approximate theory is derived for an elastic circular rod with nonuniform cross section. Three coupled equations taking into account the longitudinal, radial and axial shear deformations and their inertias are obtained as an extension of the Mindlin–McNiven theory to the case of nonuniform rods.

Responses of both the semi-infinite rod and finite rod with elastic end support subjected to either a step or a pulse loading are studied by the method of characteristics. Calculated results such as stresses vs. time for different stations along the rod and stresses as functions of distances for instants of time are presented and compared for several cases. The geometrical effect of the variation of section on the stresses and the effect of the elastic support on the reflection and propagation of the stress waves are deduced. Predicted and measured results are compared.

1. INTRODUCTION

ALTHOUGH the problem of elastic wave propagation in a rod with nonuniform cross section has been a subject of interest and investigation for decades, the existing literature is not, by far, as broad and extensive as that for rods with uniform cross section [1]. Due to the difficulty and complexity of solving the "exact" equations of motion from the three-dimensional theory of elasticity, approximations have often been made either in the form of the governing equations or in the method of solutions. A simple approach is to modify the classical one-dimensional longitudinal wave equation for a uniform rod by taking into account the variation of area or elastic modulus along the rod. The equation so obtained may be called the classical one-dimensional equation for rods with nonuniform impedence [2], or the "Webster" horn equation [3], of which extensive studies have been made [4–6]. The same theory has also attracted much attention in other fields for its practical interest, such as in the design of resonant transducers or ultrasonic concentraters in acoustics and in the study of nonuniform electric transmission lines [7].

A parallel approach to the classical one-dimensional theory was to replace the conical section of the rod by a series of thin discrete cylinders [4], based on which a numerical method had been developed [8].

It is well known that the accuracy of the classical one-dimensional equation is limited to thin rods with small changes of area and to waves which are long compared to the radius. Thus for moderate change of area or for shorter wave lengths, modifications are necessary. Chehil and Heaps [9] took into account the effect of lateral motion and obtained the longitudinal equation of motion through the use of the variational principle. A similar equation with the inclusion of lateral inertia and shear was also obtained by Martin [10].

The present paper presents a new theory. A system of three equations of motion is derived which takes into account longitudinal as well as radial and axial shear

† Consultant, Research Department, Grumman Aerospace Corporation, Bethpage, New York.

deformations and their inertias. It is an extension of the Mindlin–McNiven theory [11] to rods with nonuniform cross section. Both semi-infinite rods and finite rods subjected to either a step or a pulse loading are studied by the method of characteristics [12, 13]. Calculated stresses are obtained and plotted for different locations as functions of time. The geometrical effect of the varying cross section on the stresses and the effect of the elastic end support on the reflection and propagation of stress waves are deduced. Predicted results by the present theory are compared with measured results.

2. GOVERNING EQUATIONS FOR RODS WITH VARIABLE CROSS SECTION

The geometry of a circular rod with variable cross section is referred to a set of cylindrical coordinate system (r, θ, z) with the z-axis coincident with the axis of the rod as shown in Fig. 1. The rod extends from $z = 0$ to $z = L$ and the radius $R = R(z)$ is a continuous function of z. The displacement components in z and r directions are u_z and u_r, respectively ($u_\theta = 0$ on account of axial symmetry). The following equations are obtained from the variational equations of motion in elasticity [14].

$$\int_v \left(\frac{\partial \sigma_z}{\partial z} + \frac{\partial \sigma_{rz}}{\partial r} + \frac{\sigma_{rz}}{r} - \rho \ddot{u}_z\right) \delta u_z \, dv = 0$$
$$\int_v \left(\frac{\partial \sigma_r}{\partial r} + \frac{\sigma_r - \sigma_\theta}{r} + \frac{\partial \sigma_{rz}}{\partial z} - \rho \ddot{u}_r\right) \delta u_r \, dv = 0 \tag{1}$$

where σ_z, σ_r, σ_θ, σ_{rz} are the stress components.

To derive a set of approximate equations for motions symmetrical with respect to the rod axis and valid for moderately high frequencies, one has to consider, in addition to the longitudinal motion, the axial shear deformation and the radial deformation. In a manner similar to the case of the uniform rod considered by Mindlin and McNiven [11], the displacement components are approximated by:

$$u_z = W(z, t) + \left(1 - \frac{2r^2}{R^2}\right) \Psi(z, t), \qquad u_r = \frac{r}{R} U(z, t). \tag{2}$$

Note that in (2) R is a function of z. By substituting (2) into (1), replacing dv by $2\pi r \, dr \, dz$, integrating with respect to r through the interval $[0, R(z)]$ and setting the coefficients of

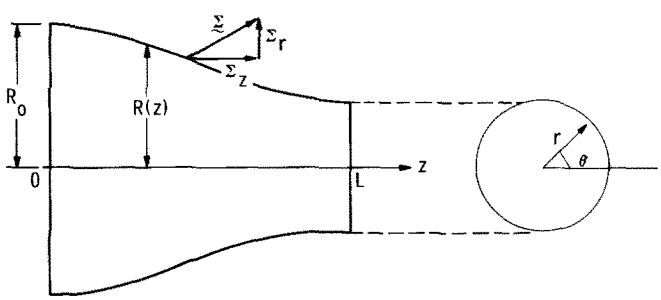

FIG. 1. Rod with variable cross section.

δW, $\delta\Psi$ and δU of the resulting equations equal to zero, one obtains the approximate stress equations of motion:

$$\begin{aligned} Q_z' + 2\left(\frac{R'}{R}\right)Q_z + \frac{2}{R}(1+R'^2)^{\frac{1}{2}}\Sigma_z &= \rho\ddot{W} \\ Q_\psi' + 4\left(\frac{R'}{R}\right)Q_\psi - 2\left(\frac{R'}{R}\right)Q_z + \frac{4}{R}Q_{rz} - \frac{2}{R}(1+R'^2)^{\frac{1}{2}}\Sigma_z &= \frac{\rho}{3}\ddot{\Psi} \\ Q_{rz}' + 3\left(\frac{R'}{R}\right)Q_{rz} - \frac{Q_r}{R} + \frac{2}{R}(1+R'^2)^{\frac{1}{2}}\Sigma_r &= \frac{\rho}{2}\ddot{U} \end{aligned} \tag{3}$$

where

$$\begin{aligned} Q_z &\equiv \frac{2}{R^2}\int_0^R \sigma_z r\,\mathrm{d}r \\ Q_\psi &\equiv \frac{2}{R^2}\int_0^R \sigma_z\left(1-\frac{2r^2}{R^2}\right)r\,\mathrm{d}r \\ Q_r &\equiv \frac{2}{R^2}\int_0^R (\sigma_r+\sigma_\theta)r\,\mathrm{d}r \\ Q_{rz} &\equiv \frac{2}{R^3}\int_0^R \sigma_{rz}r^2\,\mathrm{d}r \end{aligned} \tag{4}$$

are the generalized stress components and

$$\begin{aligned} \sum_z &= [\sigma_{rz} - R'\sigma_z]_{r=R}/(1+R'^2)^{\frac{1}{2}} \\ \sum_r &= [\sigma_r - R'\sigma_{rz}]_{r=R}/(1+R'^2)^{\frac{1}{2}} \end{aligned} \tag{5}$$

are the exact expressions for the z and r components, respectively, of the surface traction on the lateral surface $r = R(z)$ as shown in Fig. 1.

The strain energy density, according to the three-dimensional theory of elasticity is:

$$\begin{aligned} E &= \tfrac{1}{2}(\sigma_z\varepsilon_z + \sigma_r\varepsilon_r + \sigma_\theta\varepsilon_\theta + 2\sigma_{rz}\varepsilon_{rz}) \\ &= \tfrac{1}{2}[\lambda(\varepsilon_z+\varepsilon_r+\varepsilon_\theta)^2 + 2\mu(\varepsilon_z^2+\varepsilon_r^2+\varepsilon_\theta^2+2\varepsilon_{rz}^2)] \end{aligned} \tag{6}$$

where λ, μ are Lamé constants and the strains are related to the displacements by

$$\begin{aligned} \varepsilon_r &= \varepsilon_\theta = \frac{U}{R} \\ \varepsilon_z &= W' + \left(1-\frac{2r^2}{R^2}\right)\Psi' + 4\frac{r^2R'}{R^3}\Psi \\ \varepsilon_{rz} &= \frac{r}{2R}\left(U' - \frac{R'}{R}U - \frac{4}{R}\Psi\right). \end{aligned}$$

Let

$$\bar{E} = \frac{2}{R^2}\int_0^R Er\,\mathrm{d}r = \frac{1}{2}\left[Q_z\left(W' + \frac{2R'}{R}\Psi\right) + Q_\psi\left(\Psi' - \frac{2R'}{R}\Psi\right) + Q_r\frac{U}{R} + Q_{rz}\left(U' - \frac{R'}{R}U - \frac{4}{R}\Psi\right)\right] \tag{7}$$

be the generalized strain energy density for the rod, which then suggests that the generalized strain components may be defined by:

$$\begin{aligned} \Gamma_z &\equiv W' + \frac{2R'}{R}\Psi \\ \Gamma_\psi &\equiv \Psi' - \frac{2R'}{R}\Psi \\ \Gamma_r &\equiv \frac{U}{R} \\ \Gamma_{rz} &\equiv U' - \frac{R'}{R}U - \frac{4}{R}\Psi. \end{aligned} \tag{8}$$

The generalized constitutive relations may be obtained by inserting (2) into the stress–displacement relations of the three-dimensional theory and integrating the resulting expressions with respect to r according to the definitions given in (4). This gives:

$$\begin{aligned} Q_z &= 2\lambda\Gamma_r + (\lambda + 2\mu)\Gamma_z, \qquad Q_\psi = \tfrac{1}{3}(\lambda + 2\mu)\Gamma_\psi \\ Q_r &= 4(\lambda + \mu)\Gamma_r + 2\lambda\Gamma_z, \qquad Q_{rz} = \tfrac{1}{2}\mu\Gamma_{rz}. \end{aligned} \tag{9}$$

The strain energy density $\bar{E}$ may then be written in terms of the generalized strain components:

$$\begin{aligned} \bar{E} &= \tfrac{1}{2}(Q_z\Gamma_z + Q_\psi\Gamma_\psi + Q_r\Gamma_r + Q_{rz}\Gamma_{rz}) \\ &= \tfrac{1}{2}(\lambda + 2\mu)\Gamma_z^2 + \tfrac{1}{6}(\lambda + 2\mu)\Gamma_\psi^2 + 2(\lambda + \mu)\Gamma_r^2 + 2\lambda\Gamma_z\Gamma_r + \tfrac{1}{4}\mu\Gamma_{rz}^2. \end{aligned} \tag{10}$$

it can readily be shown that the generalized stress components are derivable from the generalized strain energy density function $\bar{E}$ by taking its first order derivatives with respect to the corresponding generalized strain components.

The kinetic energy density of the three-dimensional theory takes the form

$$T = \frac{\rho}{2}(\dot{u}_z^2 + \dot{u}_r^2).$$

Similarly one defines the generalized kinetic energy density for the rod:

$$\bar{T} \equiv \frac{2}{R^2}\int_0^R Tr\,\mathrm{d}r = \frac{\rho}{2}(\dot{W}^2 + \tfrac{1}{3}\dot{\Psi}^2 + \tfrac{1}{2}\dot{U}^2) \tag{11}.$$

The generalized equations of motion (3) may now be considered as being obtained by inserting (10) and (11) into the equations of the variational principle.

It was stated in Ref. [11] that because the assumed displacement functions are not exact, the expressions for the energy functions contain some inaccuracies. To compensate these, four correction factors K_1, K_2, K_3, K_4 are introduced such that Γ_r and Γ_{rz} in $\bar{E}$ are replaced by $K_1\Gamma_r$ and $K_2\Gamma_{rz}$, respectively, while $\dot{U}$ and $\dot{\Psi}$ in $\bar{T}$ are replaced by $K_3\dot{U}$ and $K_4\dot{\Psi}$, respectively. These four correction factors were obtained by matching the frequency dispersion curves of the infinite, uniform rod with those from Pochhammer's exact solution [15]. The values of these factors so obtained depend on the value of Poisson's ratio. In the case of nonuniform rods, they also depend upon the variation of the cross section, such as the slope of the rod radius: R'. This dependence could be investigated if a frequency spectrum could be found for the present case and if an exact solution exists which may be used for comparison. In lack of these informations, we are not able to obtain a rigorous analysis of the influence of the change of radius on the correction factors. However, when the slope of the radius is small, the correction factors derived for uniform rods should be applicable with good accuracy. Hence the same ones are employed here with the anticipation that for moderate slope of the rod radius, the errors will not be significant.

In what follows it is more convenient to express the equations in terms of dimensionless quantities. Let

$$x = \frac{z}{R_0}, \qquad a = \frac{R}{R_0}, \qquad l = \frac{L}{R_0}, \qquad w = \frac{W}{R_0}, \qquad \psi = \frac{\Psi}{R_0}, \qquad u = \frac{U}{R_0}$$

be the dimensionless lengths and displacements, $R_0 = R(0)$; let

$$P_z = \frac{Q_z}{\mu}, \qquad P_\psi = \frac{Q_\psi}{\mu}, \qquad P_r = \frac{Q_r}{\mu}, \qquad P_{rz} = \frac{Q_{rz}}{\mu}, \qquad S_z = \frac{\Sigma_z}{\mu}, \qquad S_r = \frac{\Sigma_r}{\mu}$$

be the dimensionless stress and surface tractions; and let

$$\tau = \frac{t}{T_0}$$

be the dimensionless time, where

$$T_0 = \frac{R_0}{\sqrt{\mu/\rho}}$$

is a reference time. One then may write, with the correction factors introduced into the energy functions,

$$\bar{E}/\mu = \tfrac{1}{2}p^2\Gamma_z^2 + \tfrac{1}{6}p^2\Gamma_\psi^2 + 2(p^2-1)K_1^2\Gamma_r^2 + 2(p^2-2)K_1\Gamma_r\Gamma_z + \tfrac{1}{4}K_2^2\Gamma_{rz}^2 \tag{12}$$

$$\bar{T}/\mu = \tfrac{1}{2}(\dot{w}^2 + \tfrac{1}{3}K_4^2\dot{\psi}^2 + \tfrac{1}{2}K_3^2\dot{u}^2). \tag{13}$$

The equations of motion are then

$$\begin{aligned}
&P_z' + \frac{2a'}{a}P_z + \frac{2}{a}(1+a'^2)^{\frac{1}{2}}S_z = \ddot{w} \\
&P_\psi' + \frac{4a'}{a}P_\psi - \frac{2a'}{a}P_z + \frac{4}{a}P_{rz} - \frac{2}{a}(1+a'^2)^{\frac{1}{2}}S_z = \tfrac{1}{3}K_4^2\ddot{\psi} \\
&P_{rz}' + \frac{3a'}{a}P_{rz} - \frac{P_r}{a} + \frac{2}{a}(1+a'^2)^{\frac{1}{2}}S_r = \tfrac{1}{2}K_3^2\ddot{u},
\end{aligned} \tag{14}$$

and for the constitutive relations the following hold:

$$\begin{aligned} P_z &= 2(p^2-2)K_1\frac{u}{a}+p^2\left(w'+\frac{2a'}{a}\psi\right) \\ P_\psi &= \frac{p^2}{3}\left(\psi'-\frac{2a'}{a}\psi\right) \\ P_r &= 4(p^2-1)K_1^2\frac{u}{a}+2(p^2-2)K_1\left(w'+\frac{2a'}{a}\psi\right) \\ P_{rz} &= \frac{K_2^2}{2}\left(u'-\frac{a'}{a}u-\frac{4}{a}\psi\right) \end{aligned} \tag{15}$$

where the primes and dots denote the partial derivatives with respect to x and τ, respectively, and

$$p^2=\frac{\lambda+2\mu}{\mu}=\frac{2(1-\nu)}{1-2\nu}$$

is a material parameter depending only on Poisson's ratio ν.

By substituting (15) into (14) one finally obtains the displacement equations of motion:

$$\begin{aligned} &w''-\frac{1}{p^2}\ddot{w}+\frac{2a'}{a}w'+\frac{2a'}{a}\psi'+\frac{2(p^2-2)K_1}{p^2a}u'+\left(2\frac{a''}{a}+2\frac{a'^2}{a^2}\right)\psi \\ &\quad+\frac{2(p^2-2)K_1a'}{p^2a^2}u+\frac{2(1+a'^2)^{\frac{1}{2}}}{p^2a}S_z=0 \\ &\psi''-\frac{K_4^2}{p^2}\ddot{\psi}-\frac{6a'}{a}w'+\frac{2a'}{a}\psi'+\frac{6K_2^2}{p^2a}u'-\left[2\frac{a''}{a}+18\frac{a'^2}{a^2}+24\frac{K_2^2}{p^2a^2}\right]\psi \\ &\quad-\frac{6[2K_1(p^2-2)+K_2^2]a'}{p^2a^2}u-\frac{6(1+a'^2)^{\frac{1}{2}}}{p^2}S_z=0 \\ &u''-\frac{K_3^2}{K_2^2}\ddot{u}-\frac{4K_1(p^2-2)}{K_2^2a}w'-\frac{4}{a}\psi'+\frac{2a'}{a}u' \\ &\quad-8\left[(p^2-2)\frac{K_1}{K_2^2}+1\right]\frac{a'}{a^2}\psi-\left[\frac{a''}{a}+\frac{2a'^2}{a^2}+\frac{8K_1^2(p^2-1)}{K_2^2a^2}\right]u \\ &\quad+\frac{4}{a}\frac{(1+a'^2)^{\frac{1}{2}}}{K_2^2}S_r=0. \end{aligned} \tag{16}$$

3. UNIQUENESS OF SOLUTIONS AND BOUNDARY CONDITIONS

To study the uniqueness of solutions, one may start by considering the rate of change of total energy in the rod. This is given by the expression:

$$\frac{1}{\mu}\int_0^l \pi R^2\left(\frac{\partial\bar{E}}{\partial\tau}+\frac{\partial\bar{T}}{\partial\tau}\right)\mathrm{d}x \tag{17}$$

where the rates of energy densities, from (10) and (11) are

$$\frac{\partial \bar{E}}{\partial \tau} = \mu\left[P_z\left(\dot{w}' + \frac{2a'}{a}\dot{\psi}\right) + P_\psi\left(\dot{\psi}' - \frac{2a'}{a}\dot{\psi}\right) + P_r\frac{\dot{u}}{a} + P_{rz}\left(\dot{u}' - \frac{a'}{a}\dot{u} - \frac{4}{a}\dot{\psi}\right)\right]$$

$$\frac{\partial \bar{T}}{\partial \tau} = \mu(\dot{w}\ddot{w} + \tfrac{1}{3}K_4^2\dot{\psi}\ddot{\psi} + \tfrac{1}{2}K_3^2\dot{u}\ddot{u}).$$

By substituting the above expressions into (17) and making use of (14) to eliminate the accelerations, one obtains, after some manipulation, the following equation:

$$\begin{aligned}\frac{1}{\mu}\int_0^l \pi R^2\left(\frac{\partial \bar{E}}{\partial \tau} + \frac{\partial \bar{T}}{\partial \tau}\right) dx = {} & R_0^3[\pi a^2(P_z\dot{w} + P_\psi\dot{\psi} + P_{rz}\dot{u})]_{x=l} \\ & - R_0^3[\pi a^2(P_z\dot{w} + P_\psi\dot{\psi} + P_{rz}\dot{u})]_{x=0} \\ & + R_0^3\int_0^l 2\pi a(1+a'^2)^{\frac{1}{2}}[S_z(\dot{w}-\dot{\psi}) + S_r\dot{u}]\,dx.\end{aligned} \tag{18}$$

In the case where the right end of the rod is attached to an elastic support, the corresponding boundary conditions are

$$\begin{aligned}P_z(l,\tau) &= -k_z w(l,\tau) \\ P_\psi(l,\tau) &= -\tfrac{1}{3}k_z\psi(l,\tau) \\ P_{rz}(l,\tau) &= -k_r u(l,\tau)\end{aligned} \tag{19}$$

where $k_z = K_z(R_0/\mu)$, $k_r = K_r(R_0/\mu)$ are the dimensionless elastic spring constants. K_z, K_r are the spring constants of the elastic support in the z and r directions respectively, with the dimensions of stress/unit length.

By substitution of (19) into the first term on the right hand side of (18) and integrating the resulting expression with respect to time from an initial time τ_0 to a later time τ, one obtains:

$$\begin{aligned}&\left[\frac{1}{\mu}\int_0^l \pi R^2(\bar{E}+\bar{T})\,dx + \pi a(l)^2 R_0^3(k_z w^2 + \tfrac{1}{3}k_z\psi^2 + k_r u^2)_{x=l}\right]_{\tau_0}^{\tau} \\ &\quad = -\int_{\tau_0}^{\tau} R_0^3\pi(P_z\dot{w} + P_\psi\dot{\psi} + P_{rz}\dot{u})_{x=0}\,d\tau \\ &\qquad + \int_{\tau_0}^{\tau} R_0^3\,d\tau\int_0^l 2\pi a(1+a'^2)^{\frac{1}{2}}[S_z(\dot{w}-\dot{\psi}) + S_r\dot{u}]\,dx.\end{aligned} \tag{20}$$

Since the constitutive relations, strain–displacement relations and equations of motion form a linear system, the difference system which corresponds to the differences of two sets of solutions in displacement, stress and strain, and the difference energy densities calculated from them must also satisfy (20). Therefore by following the usual argument based on the positive definiteness of $\bar{E}$, $\bar{T}$ and $(k_z w^2 + \frac{1}{3}k_z\psi^2 + k_r u^2)_{x=l}$, the sufficient conditions for a unique solution are:

(i) Specification of the initial condition of w, ψ, u and $\dot{w}$, $\dot{\psi}$, $\dot{u}$ throughout the rod.

(ii) Specification of one member of each of the product $P_z w$, $P_\psi\psi$ and $P_{rz}u$ at the left end of the rod (usual displacement or traction end).

(iii) The stress and displacement components satisfying the elastic relations (19) at the end of the rod (elastically supported end).

(iv) Specification of one member of each of the product $S_z(w-\psi)$ and $S_r u$ throughout the rod.

In this paper, the rod is free of tractions on the lateral surface $r = R(z)$ so that $S_r = S_z = 0$. In case the rod is finite the right end of it is supported elastically in the z direction and is free to move in the r direction so that $k_r = 0$ in (19). At the left end, the rod is subjected to a prescribed axially compressive force and the end surface remains plane. The end conditions at $x = 0$ are therefore:

$$\begin{aligned} P_z(0,\tau) &= -f(\tau) \qquad \text{for } \tau > 0 \\ &= 0 \qquad\quad\ \text{for } \tau \leq 0 \\ P_{rz}(0,\tau) &= 0 \\ \psi(0,\tau) &= 0 \end{aligned} \tag{21}$$

where $f(\tau)$ is a prescribed function.

Initially the rod is free of stresses and stationary, thus:

$$\begin{aligned} w(x,0) = \psi(x,0) = u(x,0) = 0 \\ \dot{w}(x,0) = \dot{\psi}(x,0) = \dot{u}(x,0) = 0. \end{aligned} \tag{22}$$

4. METHOD OF CHARACTERISTICS

The system of second order partial differential equations (16) with proper initial and boundary conditions (19), (21) and (22) can be solved by employing the method of characteristics [12, 13]. The general form of the equations which may be solved by this method is:

$$u_i'' - \frac{1}{c_i^2}\ddot{u}_i = \alpha_{ij}u_j + \beta_{ij}u_j' \qquad (i = 1, 2, \ldots, n) \tag{23}$$

where c_i, α_{ij}, β_{ij} are continuous functions of x. The summation convention does not apply to the index i in (23)–(26).

The characteristic lines in the $x-\tau$ plane are

$$\frac{\mathrm{d}x}{\mathrm{d}\tau} = \pm c_i \tag{24}$$

along which the differential equations take canonical forms

$$\mathrm{d}(u_i') \mp \frac{1}{c_i}\mathrm{d}(\dot{u}_i) = (\alpha_{ij}u_j + \beta_{ij}u_j')\,\mathrm{d}x. \tag{25}$$

The variables u_i must be continuous, but their derivatives may undergo finite jumps across the characteristics. These are given by the decay equations

$$[u_i'] = A_i c_i^{-\frac{1}{2}} \exp\left(\frac{1}{2}\int \beta_{ii}\,\mathrm{d}x\right)$$
$$[\dot{u}_i] = \mp A_i c_i^{\frac{1}{2}} \exp\left(\frac{1}{2}\int \beta_{ii}\,\mathrm{d}x\right) \tag{26}$$

where the symbol $[\phi]$ represents the difference of ϕ just behind a characteristic line from that just ahead of it and A_i are constants to be determined by initial and boundary conditions. In (24)–(26) the selection of the upper or the lower signs must be consistent.

Written in the form of (23), the displacement equations of motion (16) become:

$$w'' - \frac{1}{c_1^2}\ddot{w} = \alpha_{12}\psi + \alpha_{13}u + \beta_{11}w' + \beta_{12}\psi' + \beta_{13}u'$$
$$\psi'' - \frac{1}{c_2^2}\ddot{\psi} = \alpha_{22}\psi + \alpha_{23}u + \beta_{21}w' + \beta_{22}\psi' + \beta_{23}u' \tag{27}$$
$$u'' - \frac{1}{c_3^2}\ddot{u} = \alpha_{32}\psi + \alpha_{33}u + \beta_{31}w' + \beta_{32}\psi' + \beta_{33}u';$$

the canonical forms of which are accordingly

$$\mathrm{d}(w') \mp \frac{1}{c_1}\mathrm{d}(\dot{w}) = (\alpha_{12}\psi + \alpha_{13}u + \beta_{11}w' + \beta_{12}\psi' + \beta_{13}u')\,\mathrm{d}x,$$

along $\mathrm{d}x/\mathrm{d}\tau = \pm c_1$,

$$\mathrm{d}(\psi') \mp \frac{1}{c_2}\mathrm{d}(\dot{\psi}) = (\alpha_{22}\psi + \alpha_{23}u + \beta_{21}w' + \beta_{22}\psi' + \beta_{23}u')\,\mathrm{d}x,$$

along $\mathrm{d}x/\mathrm{d}\tau = \pm c_2$,

$$\mathrm{d}(u') \mp \frac{1}{c_3}\mathrm{d}(\dot{u}) = (\alpha_{32}\psi + \alpha_{33}u + \beta_{31}w' + \beta_{32}\psi' + \beta_{33}u')\,\mathrm{d}x,$$

along $dx/d\tau = \pm c_3$, where

$$c_1^2 = p^2, \qquad c_2^2 = \frac{p^2}{K_4^2}, \qquad c_3^2 = \frac{K_2^2}{K_3^2},$$

$$\alpha_{12} = -\left(\frac{2a''}{a} + \frac{2a'^2}{a^2}\right), \qquad \alpha_{13} = -\frac{2(p^2-2)K_1 a'}{p^2 a^2},$$

$$\alpha_{22} = \frac{2a''}{a} + 18\frac{a'^2}{a^2} + 24\frac{K_2^2}{a^2 p^2}, \qquad \alpha_{23} = \frac{6[2K_1(p^2-2)+K_2^2]a'}{p^2 a^2}, \tag{28}$$

$$\alpha_{32} = \frac{8}{a^2}\left[(p^2-2)\frac{K_1}{K_2^2} + 1\right], \qquad \alpha_{33} = \frac{a''}{a} + 2\frac{a'^2}{a^2} + \frac{8K_1^2(p^2-1)}{K_2^2 a^2},$$

$$\beta_{11} = -2\frac{a'}{a}, \qquad \beta_{12} = -2\frac{a'}{a}, \qquad \beta_{13} = -\frac{2(p^2-2)K_1}{p^2 a^2},$$

$$\beta_{21} = 6\frac{a'}{a}, \qquad \beta_{22} = -2\frac{a'}{a}, \qquad \beta_{23} = -\frac{6K_2^2}{p^2 a},$$

$$\beta_{31} = \frac{4K_1(p^2-2)}{K_2^2 a}, \qquad \beta_{32} = \frac{4}{a}, \qquad \beta_{33} = -2\frac{a'}{a}.$$

The characteristics $dx/d\tau = \pm c_1, \pm c_2, \pm c_3$ represent the three wave speeds of the motion in the rod. For a reasonable range of Poisson's ratio, one may assume that

$$c_1^2 > c_2^2 > c_3^2.$$

There are three characteristics emanating from the loading end of the rod at the instant of loading, which are marked by S_1, S_2, S_3 in Fig. 2. The first characteristic line S_1 is the first wave front generated from the end which distinguishes a domain at rest from a domain in motion. The condition just behind this wave front is the initial condition for the

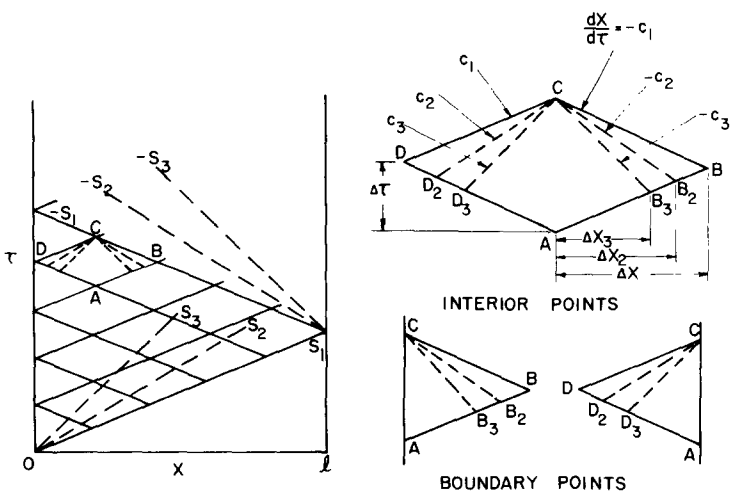

FIG. 2. Characteristic network.

numerical calculation along the characteristics. This can be obtained by considering the decay equation along S_1.

With β_{ij} given previously and the initial and the boundary conditions at the loading end incorporated, the decay equations (26) give:

$$\begin{aligned} [w'] &= -\frac{f(0)}{p^2 a}, & [\dot{w}] &= \frac{c_1 f(0)}{p^2 a} && \text{along } S_1, \\ [\psi'] &= 0, & [\dot{\psi}] &= 0 && \text{along } S_2, \\ [u'] &= 0, & [\dot{u}] &= 0 && \text{along } S_3. \end{aligned} \tag{29}$$

It is clear that discontinuities may occur only along S_1. Since the initial state of the rod is given by (22), the conditions just behind the first wave front are:

$$\begin{aligned} w' &= -\frac{f(0)}{p^2 a}, & \psi' &= 0, & u' &= 0, \\ \dot{w} &= \frac{c_1 f(0)}{p^2 a}, & \dot{\psi} &= 0, & \dot{u} &= 0. \end{aligned} \tag{30}$$

These conditions are non-zero only when $f(0) \neq 0$.

Along the first three reflected wave fronts from the right boundary, marked by $-S_1$, $-S_2$, $-S_3$ in Fig. 2, (26) also gives three jump conditions which, after substitution in the corresponding initial and boundary conditions reduce to

$$\begin{aligned} [w'] &= \frac{f(0)}{p^2 a} & [\dot{w}] &= \frac{c_1 f(0)}{p^2 a} && \text{along } -S_1, \\ [\psi'] &= 0, & [\dot{\psi}] &= 0 && \text{along } -S_2, \\ [u'] &= 0, & [\dot{u}] &= 0 && \text{along } -S_3. \end{aligned} \tag{31}$$

5. NUMERICAL ANALYSIS

Also shown in Fig. 2 are the characteristics drawn in discrete lines. Only the first families, $\mathrm{d}x/\mathrm{d}\tau = \pm c_1$, are shown as continuous lines, while the second and the third families with $\mathrm{d}x/\mathrm{d}\tau = \pm c_2, \pm c_3$ appear in broken segments. This is desirable because there are no finite jumps across the second and third families of characteristics. A typical element of the meshes of finite differences is represented by the diamond-shaped domain $ABCD$, whose diagonal lengths are $2\Delta x$ and $2\Delta\tau$ in the x and τ directions, respectively. The lines of the characteristics are shown in the enlarged diagram on the right, in which the increments Δx_2 and Δx_3 are given by

$$\Delta x_2 = \frac{2c_2}{c_1 + c_2}\Delta x, \qquad \Delta x_3 = \frac{2c_3}{c_1 + c_3}\Delta x.$$

The characteristics of boundary points are also shown in the same figure.

The values of the quantities at C can be calculated from those at A, B, B_2, B_3, D, D_2, and D_3, where the values at B_2, B_3, D_2, and D_3 are in turn obtained by interpolation from those at A, B and D.

The implicit method with backward-differences in τ is used in setting up the difference equations. Usually, the implicit method involves solving a system of simultaneous equations, which is not very practical if the number of equations is large. In the present case, the number is only two or three. The numerical method is described in the following, the convergence of which has been proved [13].

If C is an interior point, the canonical forms (28) give the following six equations along the characteristics:

along $\mathrm{d}x/\mathrm{d}\tau = c_1$,

$$w'(C)-w'(D)-\frac{1}{c_1}[\dot{w}(C)-\dot{w}(D)]$$
$$= [\alpha_{12}\psi(C)+\alpha_{13}u(C)+\beta_{11}w'(C)+\beta_{12}\psi'(C)+\beta_{13}u'(C)]\Delta x, \tag{32a}$$

along $\mathrm{d}x/\mathrm{d}\tau = c_2$,

$$\psi'(C)-\psi'(D_2)-\frac{1}{c_2}[\dot{\psi}[(C)-\dot{\psi}(D_2)]$$
$$= [\alpha_{22}\psi(C)+\alpha_{23}u(C)+\beta_{21}w'(C)+\beta_{22}\psi'(C)+\beta_{23}u'(C)]\Delta x_2, \tag{32b}$$

along $\mathrm{d}x/\mathrm{d}\tau = c_3$,

$$u'(C)-u'(D_3)-\frac{1}{c_3}[\dot{u}(C)-\dot{u}(D_3)]$$
$$= [\alpha_{32}\psi(C)+\alpha_{33}u(C)+\beta_{31}w'(C)+\beta_{32}\psi'(C)+\beta_{33}u'(C)]\Delta x_3, \tag{32c}$$

along $\mathrm{d}x/\mathrm{d}\tau = -c_1$,

$$w'(C)-w'(B)+\frac{1}{c_1}[\dot{w}(C)-\dot{w}(B)]$$
$$= -[\alpha_{12}\psi(C)+\alpha_{13}u(C)+\beta_{11}w'(C)+\beta_{12}\psi'(C)+\beta_{13}u'(C)]\Delta x, \tag{33a}$$

along $\mathrm{d}x/\mathrm{d}\tau = -c_2$,

$$\psi'(C)-\psi'(B_2)+\frac{1}{c_2}[\dot{\psi}(C)-\dot{\psi}(B_2)]$$
$$= -[\alpha_{22}\psi(C)+\alpha_{23}u(C)+\beta_{21}w'(C)+\beta_{22}\psi'(C)+\beta_{23}u'(C)]\Delta x_2, \tag{33b}$$

along $\mathrm{d}x/\mathrm{d}\tau = -c_3$,

$$u'(C)-u'(B_3)+\frac{1}{c_3}[\dot{u}(C)-\dot{u}(B_3)]$$
$$= -[\alpha_{32}\psi(C)+\alpha_{33}u(C)+\beta_{31}w'(C)+\beta_{32}\psi'(C)+\beta_{33}u'(C)]\Delta x_3, \tag{33c}$$

where all the α's and β's take their values at C. These are supplemented by three equations along $\mathrm{d}x/\mathrm{d}\tau = 0$:

$$\begin{aligned} w(C) &= w(A)+2\Delta\tau\dot{w}(C) \\ \psi(C) &= \psi(A)+2\Delta\tau\dot{\psi}(C) \\ u(C) &= u(A)+2\Delta\tau\dot{u}(C). \end{aligned} \tag{34}$$

Equations (32)–(34) constitute a set of nine equations in terms of w, ψ, u, w', ψ', u', $\dot{w}$, $\dot{\psi}$, $\dot{u}$ at C.

After some manipulation, they may be reduced to a set of two simultaneous equations involving only $\dot{\psi}$ and $\dot{u}$, which may be solved easily.

If C is a left boundary point, the three equations of (32) are replaced by the boundary condition (21), which, combined with (15), gives

$$\begin{aligned} 2(p^2-2)K_1u(C)+p^2w'(C) &= -f(C) \\ \psi(C) &= 0 \\ u'(C)-a'(0)u(C) &= 0. \end{aligned} \tag{35}$$

A system of two simultaneous equations in terms of ψ' and $\dot{u}$ may be obtained.

If C is a right boundary point, (33) should be replaced by (19) with $k_r = 0$, which combining with (15) becomes

$$\begin{aligned} -k_zw(C) &= \frac{2(p^2-2)K_1}{a(l)}u(C)+p^2\left[w'(C)+\frac{2a'(l)}{a(l)}\psi(C)\right] \\ -k_z\psi(C) &= p^2\left[\psi'(C)-\frac{2a'(l)}{a(l)}\psi(C)\right] \\ u'(C)-\frac{a'(l)}{a(l)}u(C)-\frac{4}{a(l)}\psi(C) &= 0. \end{aligned} \tag{36}$$

In this case the system may be reduced to three simultaneous equations in $\dot{w}$, $\dot{\psi}$ and $\dot{u}$.

6. NUMERICAL RESULTS

The transient stress wave propagations in rods with variable cross sections are investigated numerically by the method of characteristics as described in Sections 4 and 5. Poisson's ratio is chosen to be 0·29 and the correction factors are $K_1 = 0{\cdot}8797$, $K_2 = 1{\cdot}1550$, $K_3 = 0{\cdot}9876$ and $K_4 = 1{\cdot}4767$ as were calculated by Kaul and McCoy [16]. The mesh size is selected for $\Delta x = 0{\cdot}04$ which gives $\Delta\tau = 0{\cdot}02175$.

Semi-infinite rods subjected to step-loading are considered first. The purpose of this is to separate the geometrical effect from the influence due to the wave reflections from the end which depends strongly on the end conditions and will be studied later in detail. Although the governing equations and numerical procedures presented earlier are applicable to any rod with "smooth and gradual" variation of cross-sectional area, for simplicity the "cylinder–cone–cylinder" type of area changes were considered; these consist of an assembly of a very short circular cylinder on the left (loading) end, a linear cone in the middle and a semi-infinite cylinder with smaller radius on the right. Three rods with different lengths for the conical portions are selected as shown in Fig. 3 in which a uniform rod is also included for comparison. The generalized axial stress at positions one and two diameters respectively from the loading end are calculated and plotted in Figs. 3(a) and (b). In all four cases, the same step-loading is applied at the left end of the rods. For a steel rod with end radius $R_0 = 3$ in., one unit of dimensionless time is equivalent to 23·7 μsec. When the first wave front, with dimensionless dilatational velocity $c_1 = [\lambda+2\mu)/\mu]^{\frac{1}{2}}$, reaches the position of consideration (at $\tau - x/c_1 = 0$), the magnitude of stress is inversely proportional

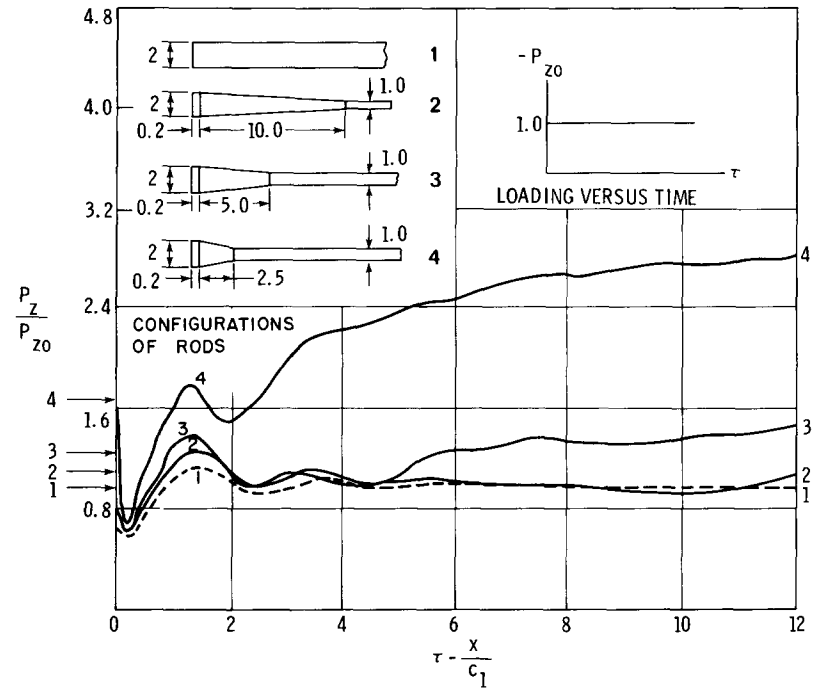

(a)

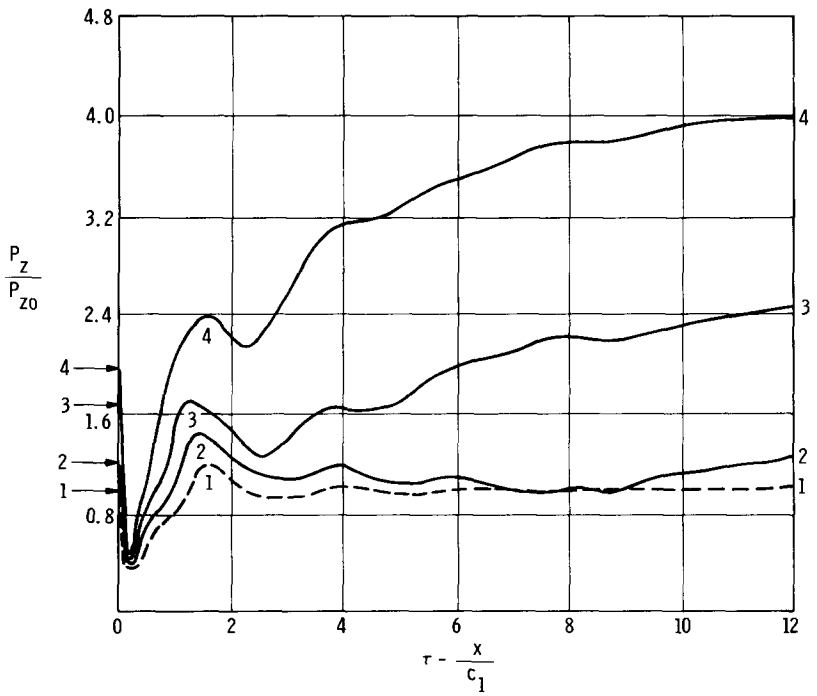

(b)

FIG. 3. Axial stress vs. time. (a) At 1 diameter from the end. (b) at 2 diameters from the end.

to the radius of the rod. This stress discontinuity is due to the propagation of the discontinuous initial value of the applied load, $f(0)$, and its magnitude along the rod is governed by the decay equations (29). After the first wave front has passed, the stress drops immediately to a much lower level and then rises to a peak, which is created essentially by the waves with bar velocity $c_0 = (E/\mu)^{\frac{1}{2}} < c_1$. After that, the stress gradually approaches its steady state value. By comparing the stresses in rods 2–4 of Fig. 3(a) with those of Fig. 3(b) one sees that the magnitude of stress increases as the cross-sectional area of the rod decreases.

Further study is made of two rods with identical end diameter and the same loading conditions, but with one rod having a shorter conical portion than the other, as shown in Fig. 4. Comparison of the stresses at a station 2·6 diameters from the loading end shows that the steeper the slope of the conical portion, the higher the stress level and the faster the rate of approach to the steady-state value.

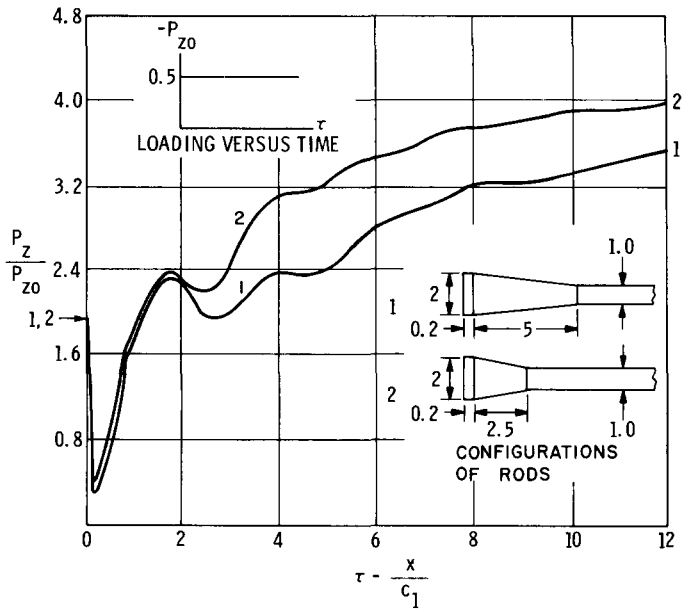

FIG. 4. Axial stress vs. time at 2·6 diameters from the end.

Calculations of the generalized axial and radial strains and axial velocity are also made. The results are similar to those of the axial stresses except that the radial strains do not have initial discontinuities when the first dilatational wave fronts arrive.

To study the effect of the end support on the reflections of stress waves from the end, a finite rod of the same "cylinder–cone–cylinder" type is considered. The boundary conditions of an elastic support at the right end ($x = l$) are given by (19) with $k_r = 0$ as explained previously. The two extreme cases for an elastic support are the free end ($k_z = 0$) and the fixed end ($k_z = \infty$). Thus by calculating the stress and velocity fields in the rod for various values of the spring constant of the support, one may investigate the effect of the stiffness of the support on the wave reflections within the rod. For a steel cone with $R_0 = 3$ in. and $\mu = 12 \times 10^6$ psi, the dimensionless value of $k_z = 1$ corresponds to a spring constant $K_z = 4 \times 10^6$ psi/in.

Figure 5(a) shows the configuration of the rod and the generalized axial stress at four positions due to a pulse loading. The elastic support at the right end has a spring constant $k_z = 1$. A larger value of the constant, $k_z = 5$, is also used and the results are shown in Fig. 5(b).

It is seen that the stress at the end of the rod with a softer support rises with a slower rate, reaches a lower peak value but lasts longer.

Figures 6(a) and (b) show the stresses of the same system as those in Figs. 5(a) and (b) but subjected to a modified step loading. Within the time period for the first wave front to travel two cycles, the stresses at the positions 2–4 are considerably raised as compared with those in Figs. 5(a) and (b). Also, the elastic support has little effect on the stress peak when the duration of loading is long enough. As may be noted in those figures, a continuous loading with a very short transition period ($\Delta\tau = 0{\cdot}2$) is chosen to replace a step loading. This eliminates the propagation of stress discontinuity at the first wave front but gives rise to little effect upon the subsequent stress states. Hence it simplifies the numerical procedure by making the consideration of the jump conditions unnecessary.

Finally, calculations are made to compare with experimental results on two specimens as obtained by Leftheris [17]. The experimental setup is outlined in Fig. 7. A "cylinder–cone–cylinder" stainless steel specimen is connected at the larger end to a 6 in. diameter, 12 in. long aluminum rod and at the smaller end to a 1 in. diameter, 288 in. long steel rod. A stress wave generator is connected to the other end of the aluminum rod. This generator produces a local, high intensity, electro-magnetic field resulting from the discharge of a capacitor bank. The electro-magnetic field then induces a stress wave which moves into the aluminum rod. One strain gauge (G_1) is mounted on the aluminum rod 1 in. from its right end, while another one (G_2) is mounted on the steel rod 48 in. from its left end. These two gauges measure the strain waves into and out of the specimen respectively, which are amplified and displayed on an oscilloscope. The steel rod is long enough so that reflection from the end has no effect within the time of consideration and the assembly may be considered as semi-infinite. The stress waves are assumed to be uniform in the aluminum rod so that the input gauge reading at G_1 may be used to determine $f(\tau)$ for the boundary condition at the left end of the specimen.

Two different shapes of specimen are tested under the same loading program so that the input data measured by the gauge G_1 for the two cases are essentially the same. Figure 8 shows the result of one of the tests. The upper trace is the input pulse of G_1, created by the stress wave generator, and the lower trace is the output strain wave at G_2. The measured axial surface strains at G_2, which is located at 48 in. from the smaller ends of the cones, as indicated in Fig. 8 together with the calculated results are plotted in Figs. 9 and 10 for the 5 in. (54·2° apex angle) and 24 in. (11·9° apex angle) cones, respectively.

Also appeared in these figures are the computed results from the classical one-dimensional theory [2, 3], referred to here as the one-mode theory in contrast with the present three-mode theory. It can be seen from Fig. 10 that the surface strain calculated from the present three-mode theory does not differ much from that of the one-mode theory for the 24 in. cone. However, for the 5 in. cone the present theory does appear to be better than the classical one-mode theory as compared with the experimental result in Fig. 9. This is in agreement with Kenner and Goldsmith's finding [18] that the analysis of the classical one-mode theory is valid for cones with an apex angle less than 30°. It is therefore reasonable to conclude that for waves with shorter wave lengths and rods with larger apex angles, the present theory is more suitable to apply.

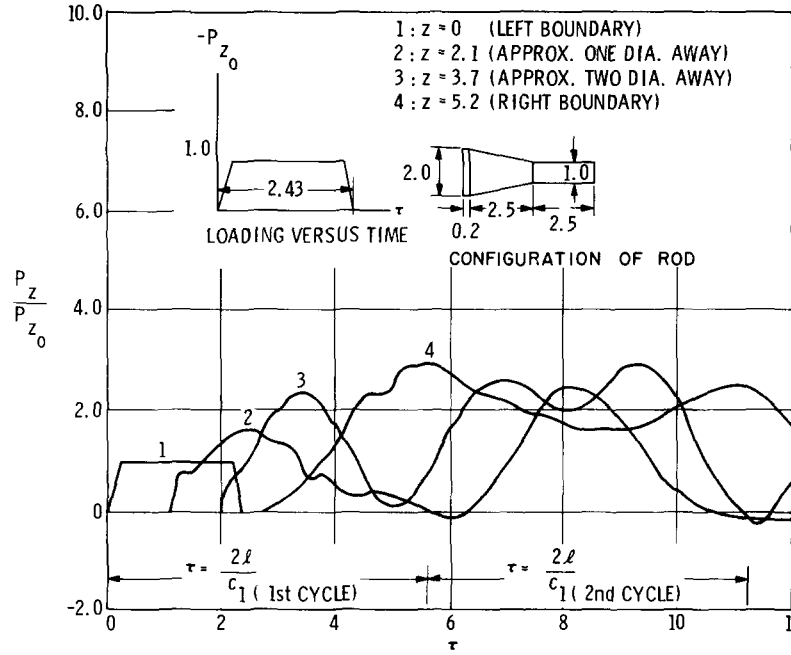

(a)

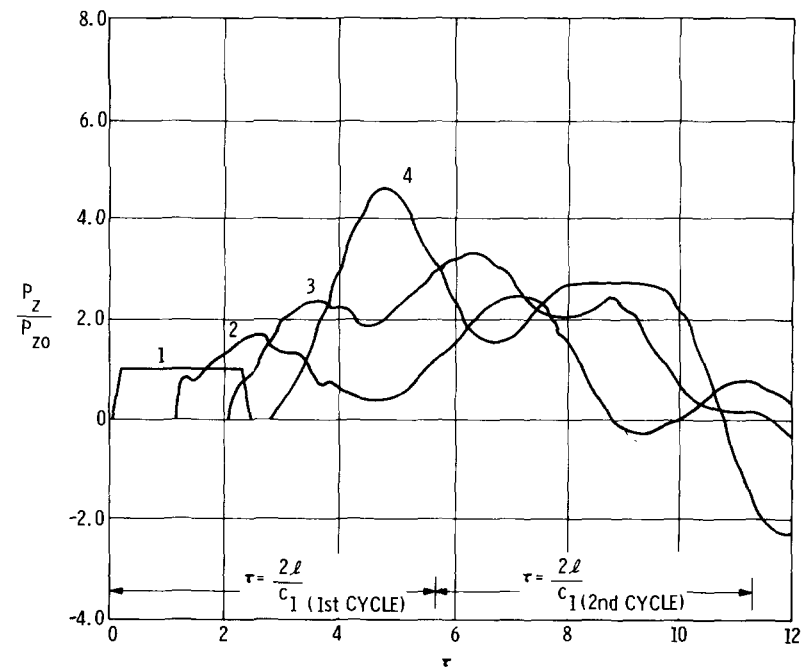

(b)

FIG. 5. Axial stress vs. time for finite rod subjected to pulse loading. (a) Soft elastic end support, $k_z = 1$. (b) Stiff elastic end support, $k_z = 5$.

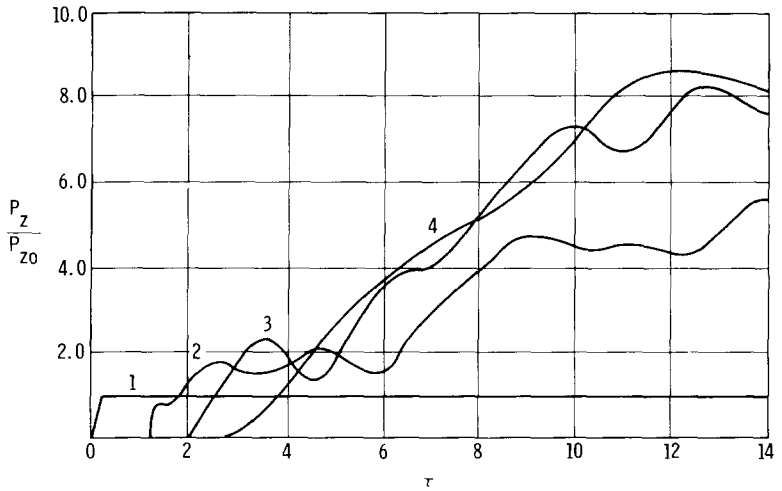

(a)

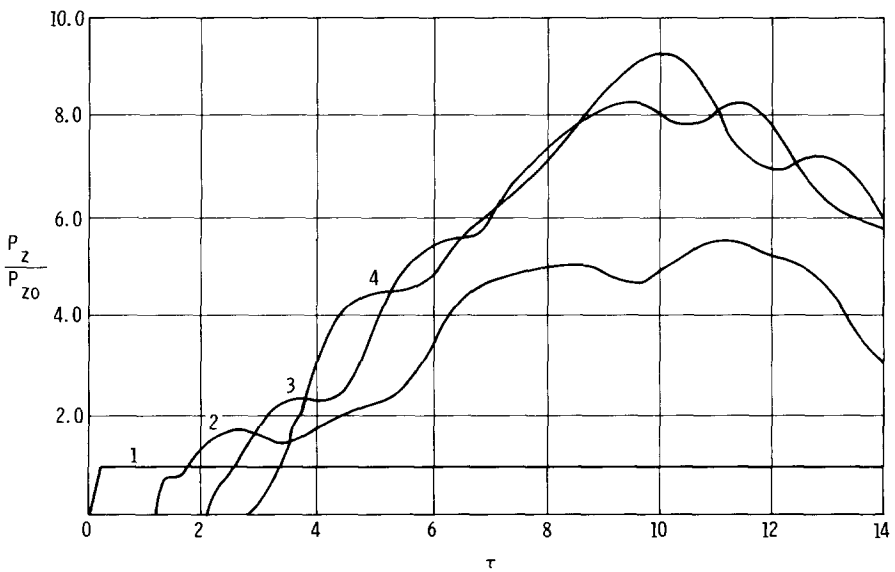

(b)

FIG. 6. Axial stress vs. time for finite rod subjected to step loading. (a) Soft elastic end support, $k_z = 1$. (b) Stiff elastic end support, $k_z = 5$.

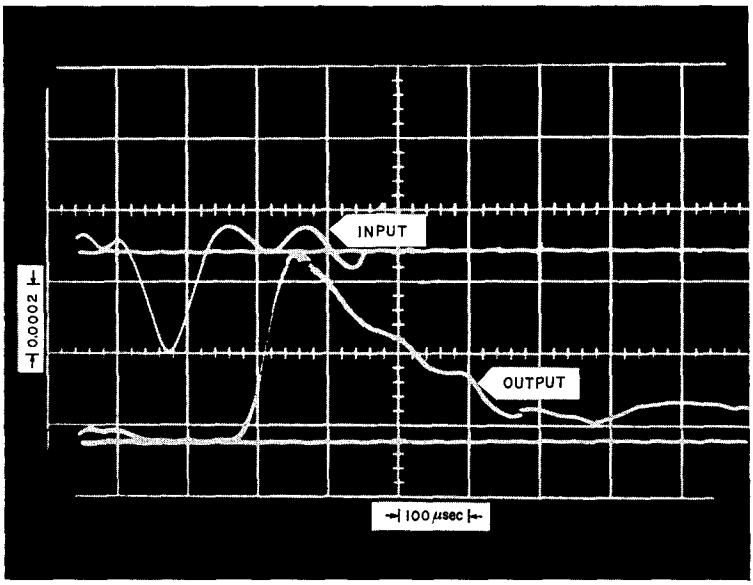

FIG. 8. Experimental result.

facing p. 478

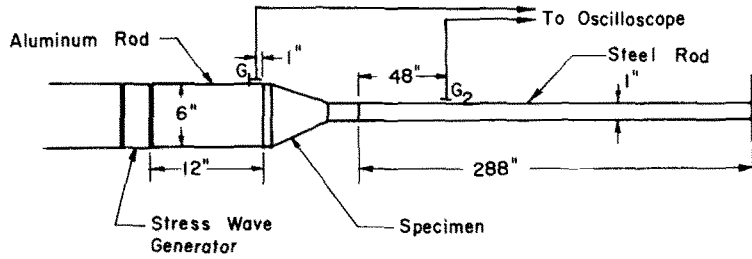

FIG. 7. Diagram of the experimental setup.

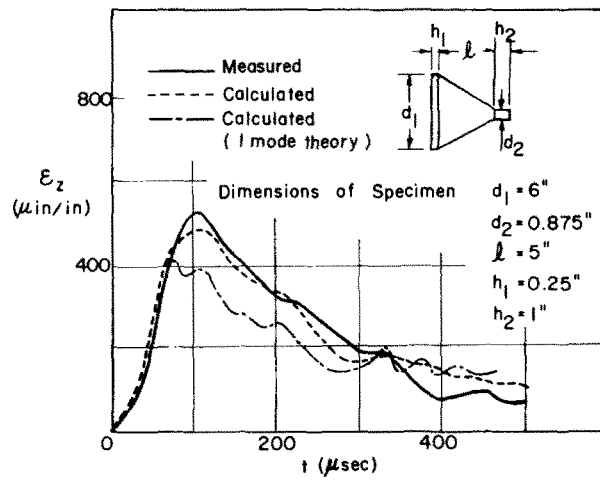

FIG. 9. Comparison of the axial strain.

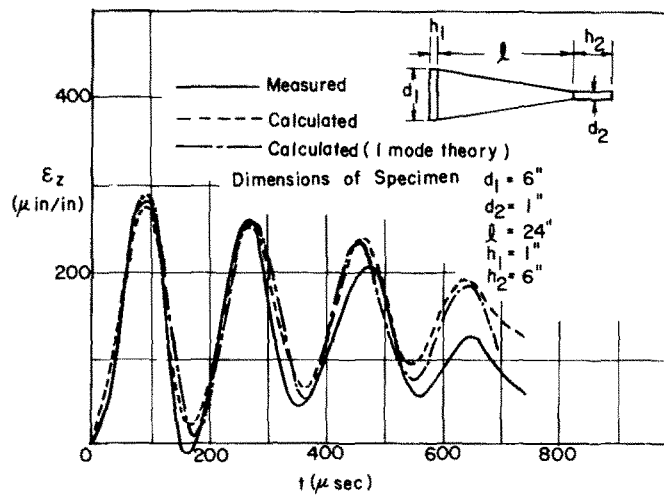

FIG. 10. Comparison of the axial strain.

REFERENCES

[1] J. Miklowitz, Elastic Wave Propagation, *Applied Mechanics Surveys*, edited by H. N. Abramson, H. Liebowitz, J. M. Crowley and S. Juhasz. Spartan (1966).
[2] J. W. S. Rayleigh, On the propagation of sound in narrow tubes of variable section. *Phil. Mag.* **31**, 89–96 (1916).
[3] G. A. Webster, Acoustic impedance and the theory of horns and the phonograph. *Proc. natl. Acad. Sci.* **5**, 275–282 (1919).
[4] L. H. Donnell, Longitudinal wave transmission and impact. *Trans. Am. Soc. Mech. Engrs* **52**, 153–167 (1930).
[5] U. S. Linholm and K. D. Doshi, Wave propagation in elastic nonhomogeneous bar of finite length. *J. appl. Mech.* **32**, 135–142 (1965).
[6] T. Y. Tsui, Wave propagation in a finite length bar with a variable cross section. *J. appl. Mech.* **35**, 824–825 (1968).
[7] E. Eisner, Complete solution of the "Webster" horn equation. *J. acoust. Soc. Am.* **41**, 1126–1146 (1967).
[8] M. Mao and D. Rader, Longitudinal stress pulse propagation in nonuniform elastic and viscoelastic bars. *Int. J. Solids Struct.* **6**, 519–538 (1970).
[9] D. S. Chehil and H. S. Heaps, Effect of lateral motion on the longitudinal vibration of bars with conical taper. *J. acoust. Soc. Am.* **43**, 540–544 (1968).
[10] G. E. Martin, On the Propagation of Longitudinal Stress Waves in Finite, Solid, Elastic Horns, Ph.D. Dissertation, University of Texas (1966).
[11] R. D. Mindlin and H. D. McNiven, Axially symmetric waves in elastic rods. *J. appl. Mech.* **27**, 145–151 (1960).
[12] P. C. Chou and R. W. Mortimer, Solution of one-dimensional elastic wave problems by the method of characteristics. *J. appl. Mech.* **34**, 745–750 (1967).
[13] Y. Mengi and H. D. McNiven, Analysis of the transient excitation of an elastic rod by the method of characteristics. *Int. J. Solids Struct.* **6**, 871–892 (1970).
[14] A. E. H. Love, *A Treatise on the Mathematical Theory of Elasticity*. Dover (1944).
[15] L. Porchhammer, On the velocity of propagation of small vibrations in an infinite, isotropic, circular cylinder. *J. Reine angew. Math.* **81**, 324–336 (1876).
[16] R. K. Kaul and J. J. McCoy, Propagation of axisymmetric waves in a circular semiinfinite elastic rod. *J. acoust. Soc. Am.* **36**, 653–660 (1964).
[17] B. P. Leftheris, private communication.
[18] V. H. Kenner and W. Goldsmith, Elastic waves in truncated cones. *Exp. Mech.* **8**, 442–449 (1968).

(*Received* 10 *January* 1972; *revised* 30 *May* 1972)

Абстракт—Решается одномерная приближенная теория для упругого круглого стержня с неравномерным поперечным сечением. Получаются три сопряженные уравнения, которые учитывают продольные, радиальные и осебые деформации сдвига и их инерции. Эти уравнения являются обобщением теории Миндлина-МакНивена для случая неоднородных стержней.

Путем метода характеристик исследуются поведения как полубесконечного стержня, так и конечного, с упругим операнием концов, подверженных действию либо скачкообразной нагрузки, или импульсивной. Для разных моментов времени даются подсчитанные результаты, такие как напряжения в зависимости от времени для разных положений вдолв стержня, в форме функций расстояния и сравниваются для некоторых случаев. Определяются зависимости напряжений от геометрического эффекта изменения сечения и зависимости отражения и распространения волн напряжений от эффекта упругого операния. Сравниваются предсказанные и измеренные результаты.